Matrix Biology 136 (2025) 22–35

Contents lists available at ScienceDirect

Matrix Biology

journal homepage: www.elsevier.com/locate/matbio

Neurocan regulates axon initial segment organization and neuronal activity

David Baidoe-Ansah [a,1], Hadi Mirzapourdelavar [a,1], Stepan Aleshin [a], Björn Hendrik Schott [b,c,d,e], Constanze Seidenbecher [b,c,f], Rahul Kaushik [a], Alexander Dityatev [a,c,g,*]

[a] German Center for Neurodegenerative Diseases (DZNE), Helmholtz Association of German Research Centers, Magdeburg, Germany
[b] Leibniz Institute for Neurobiology (LIN), Magdeburg, Germany
[c] Center for Behavioral Brain Sciences (CBBS), Magdeburg, Germany
[d] Department of Psychiatry and Psychotherapy, University Medical Center, Göttingen, Germany
[e] German Center for Neurodegenerative Diseases (DZNE), Göttingen, Germany
[f] Center for Intervention and Research on Adaptive and Maladaptive Brain Circuits Underlying Mental Health (C-I-R-C), Jena-Magdeburg-Halle, Germany
[g] Medical Faculty, Otto-von-Guericke University, Magdeburg, Germany

ARTICLE INFO

Keywords:
Extracellular matrix
Perineuronal net
Neurocan
Neuronal excitability
Synaptic plasticity

ABSTRACT

The neural extracellular matrix (ECM) accumulates in the form of perineuronal nets (PNNs), particularly around fast-spiking GABAergic interneurons in the cortex and hippocampus, but also around synapses and in association with the axon initial segments (AIS) and nodes of Ranvier. Increasing evidence highlights the role of Neurocan (Ncan), a brain-specific component of ECM, in the pathophysiology of neuropsychiatric disorders like bipolar disorder and schizophrenia. Ncan localizes at PNNs, perisynaptically, and at the nodes of Ranvier and the AIS, highlighting its potential role in regulating axonal excitability. Here, we used knockdown and knockout approaches in mouse primary cortical neurons in combination with immunocytochemistry, Western blotting and electrophysiological techniques to characterize the role of Ncan in the organization of PNNs and AISs and regulation of neuronal activity. We found that reduced Ncan levels led to remodeling of PNNs around neurons via upregulation of aggrecan mRNA and protein levels, increased expression of activity-dependent c-Fos and FosB genes and elevated spontaneous synaptic activity. The latter correlated with increased levels of ankyrin-G in the AIS, particularly in excitatory neurons, and with the elevated expression of $Na_v1.6$ channels. Our results suggest that Ncan regulates the expression of key proteins in PNNs and AISs and provide new insights into its role in fine-tuning neuronal functions.

Introduction

Neuronal excitability and synaptic communication in the central nervous system (CNS) rely on the initiation of action potentials (APs) at the axon initial segment (AIS) [1,2] and its propagation along the axon towards the synaptic terminals. The initiation and propagation of APs are facilitated by the aggregation of voltage-gated sodium (Na_v) and potassium channels [3]. Interestingly, Na_v channels cluster at densities shown to be more than 50-fold higher in the AIS as compared to dendrites [4]. At the AIS, different Na_v isoforms have been identified, including $Na_v1.1$, $Na_v1.2$, and $Na_v1.6$ [5,6], which serve as the key ion channels in regulating neuronal excitability. These channels are distributed at distinct locations along the AIS, with the proximal region mainly containing $Na_v1.1$ and $Na_v1.2$ channels, whereas $Na_v1.6$ channels are enriched at the distal AIS and the node of Ranvier [7,8]. The clustering of $Na_v1.2$ and $Na_v1.6$ is regulated differently [9], and they also differ functionally. While $Na_v1.6$ initiates APs in excitatory and inhibitory neurons, $Na_v1.2$ controls AP transmission, especially the backpropagation of APs [8]. The clustering and distribution of Na_v depend on the adaptor protein ankyrin G (AnkG) [10]. Structurally, AnkG regulates the localization and diffusion of ion channels [4] and other AIS proteins, including the cell adhesion molecule Neurofascin-186 and βIV-spectrin [11,12].

The AIS is also enriched in some extracellular matrix (ECM) molecules [13–15]. The neural ECM generally comprises hyaluronic acid, proteoglycans, and a variety of other glycoproteins [16], and it exists in

* Corresponding author at: German Center for Neurodegenerative Diseases (DZNE), Leipziger Str. 44, Haus 64, Magdeburg 39120, Germany.
E-mail address: alexander.dityatev@dzne.de (A. Dityatev).
[1] David Baidoe-Ansah and Hadi Mirzapourdelavar contributed equally to this work.

https://doi.org/10.1016/j.matbio.2025.01.001
Received 17 November 2024; Received in revised form 31 December 2024; Accepted 6 January 2025
Available online 7 January 2025

diffuse forms as perisynaptic and interstitial ECM or in more dense forms as periaxonal coats and perineuronal nets (PNNs) [15,17,18]. PNNs mostly surround inhibitory neuronal cell bodies and proximal dendrites. They are made up of chondroitin sulfate proteoglycans (CSPGs) attached to the hyaluronic acid backbone, stabilized by link proteins and the glycoprotein Tenascin-R (TnR) [19]. CSPGs found in PNNs are aggrecan (Acan), brevican (Bcan), neurocan (Ncan), and versican (Vcan), which also occur in varying degrees of expression at the AIS [11]. Bcan, Vcan, and TnR are highly enriched at the AIS whereas Acan and Ncan are expressed in a lesser amount [11,20]. The AIS ECM is expressed as prominent axonal coats, more uniform than PNNs having a mesh-like appearance with "holes", and it can be more broadly found in association with both PNN-positive and -negative neurons [11,21].

Several studies have explored the role of neural ECM composition in neuronal excitability. For instance, digestion of chondroitin sulfates with chondroitinase ABC modulates the excitability of parvalbumin (Pvalb)-expressing interneurons [22,23]. In contrast, the digestion of heparan sulfates with heparinase reduces the excitability of excitatory neurons and downregulates AnkG at the AIS [24] in a calcium/calmodulin kinase II-dependent manner [25]. Knockdown of *Bcan* in Pvalb--positive interneurons reduced their excitability via modifying the clustering of potassium channels [26]. These studies suggest that ECM molecules are essential for regulating neuronal excitability. Ncan has recently received considerable attention as the human *NCAN* gene has been identified as a genetic risk factor for bipolar disorder and the manic phenotype [27,28], and for schizophrenia [29]. Furthermore, data from animal models and patients show dysregulation of *NCAN* expression in several CNS disorders associated with abnormalities in neuronal and network activity, such as epilepsy [30], depression [31], or Alzheimer's disease [32]. In healthy humans, the *NCAN* psychiatric risk variant rs1064395 has been associated with hippocampus-dependent memory function and prefrontal gray matter density [33–35], but the mechanistic role played by *NCAN* has not been elucidated.

Considering the link between *NCAN* and prefrontal gray matter density, we decided to study Ncan functions in murine cultures of dissociated cortical neurons, particularly as this two-dimensional experimental system is advantageous for the detailed analysis of AIS organization [24]. This choice of the experimental system is also supported by the mentioned associations between *NCAN* and psychiatric disorders and data showing (i) decreased frontal cortical volume in mania, (ii) a failure in the prefrontal cortex (PFC) modulation of anterior limbic structures such as the amygdala resulting in emotional dysregulation in bipolar disorder and (iii) inefficient cognitive information processing in the PFC in schizophrenia [36,37].

Considering the pattern of Ncan expression, we asked if knockout and/or knockdown of *Ncan* will affect PNNs and the associated Pvalb-expressing neurons or the organization of AIS in excitatory or inhibitory neurons. The knockdown approach was employed to avoid activation of the potential genetic compensatory mechanisms quite common for knockout models [38,39]. We knocked down *Ncan* using AAVs to express one of two Ncan shRNAs in mouse primary cortical neurons from DIV 7 to DIV 21 and investigated the effects of Ncan depletion on the expression of various ECM components of PNNs and AISs using RT-qPCR, Western blotting and immunocytochemistry. Our analysis revealed complex changes in the expression of PNN components and retarded maturation of Pvalb-expessing interneurons on the one hand and elevation of AnkG expression, particularly in AISs of excitatory neurons on the other hand. Electrophysiological recordings demonstrated how these molecular alterations are translated into elevated neuronal activity.

Results

Ncan depletion results in dysregulated expression of PNN components in vitro

To thoroughly dissect Ncan functions, we studied the effects of attenuated Ncan expression *in vitro* by generating two AAVs encoding shRNAs targeting the *Ncan* mRNA and evaluated fold changes in mRNA and protein levels by RT-qPCR and ICC, respectively (Fig. 1A). Quantification of *Ncan* expression was conducted in dissociated cortical neurons infected with Ncan shRNA1 or shRNA2, control vectors (Ctrl), and *Ncan* KO neurons that were infected with control vectors (*Ncan* KO) at DIV7 for a duration of 14 days. Following normalization to the internal control, *Gapdh*, our findings indicated that shRNA1 led to an approximate 50 % reduction in *Ncan* expression, while shRNA2 resulted in a more prominent 90 % reduction compared to the Ctrl condition (Fig. 1B). As expected, *Ncan* transcripts were not detectable in *Ncan* KO neurons (Fig. 1B). Subsequently, we examined the specificity of our constructs and their impact on the expression of other PNN molecules. Notably, the reduction of *Ncan* was associated with upregulated *Acan* mRNA levels in both shRNA1- and shRNA2-expressing groups, as well as in *Ncan* KO neurons (Fig. 1B). However, the mRNA levels of another PNN proteoglycan, *Bcan*, were significantly reduced in *Ncan* KO cultures and showed a similar tendency in Ncan depleted cultures. Moreover, a decreased expression of *Hapln1* (Hyaluronan and Proteoglycan Link Protein 1), was observed in shRNA1-expressing neurons, while *Hapln1* expression was upregulated in both shRNA2 and *Ncan* KO neurons (Fig. 1B). Intriguingly, reduced *Ncan* levels were found to be associated with a corresponding decrease in mRNA levels of *Hapln4*. Conversely, *Ncan* KO neurons showed upregulation of *Hapln4* mRNA levels (Fig. 1B).

To confirm these findings at the protein level, quantification of Acan protein was done in shRNA1- and shRNA2-treated cells as well as in *Ncan* KO neurons (Fig. 1C,D). Interestingly, Acan levels increased significantly in the shRNA1 and shRNA2 groups relative to Ctrl in both Western blot and ICC analyses (Fig. 1 D–F). To validate the specificity of shRNA constructs, we performed a Western blot analysis of *Ncan* KO neurons treated with shRNA1 or shRNA2. As expected, no significant changes in Acan and Bcan were induced in these experiments (Fig. 1C).

Expression analysis for two developmentally regulated genes, *Pvalb* and Potassium voltage-gated channel subfamily C member 1 (*Kcnc1*), which are selectively expressed in fast-spiking interneurons associated with PNNs, revealed their decreased/retarded expression in shRNA1- and shRNA2-expressing neurons. In contrast, the expression levels in *Ncan* KO neurons were similar to Ctrl (Fig. 2A). Reduced expression of Kcnc1 channels known to be responsible for fast repolarization of these cells [41] may reduce the frequency of interneuronal firing and result in reduced *Pvalb* expression.

Effects of Ncan knockdown on neuronal activity and plasticity-dependent gene expression

Analysis for the neuronal activity markers c-Fos and FosB showed elevated mRNA levels of *Fos* and *Fosb* in all treated groups compared to the Ctrl group (Fig. 2B). Consistent with mRNA levels, the protein level of FosB was increased, suggesting elevated overall neuronal activity following Ncan depletion (Fig. 2C). Next, we investigated the effects of Ncan depletion on changes in gene expression after induction of synaptic plasticity. We used glycine-induced chemical long-term potentiation (GI-LTP), the global form of LTP, as it has been shown to mediate similar cellular processes as tetanus-induced LTP [42]. Mature cortical cultures (DIV21) infected with Ncan shRNA and Ctrl at DIV7 were exposed to ACSF (basal condition) or ACSF supplemented with glycine to facilitate

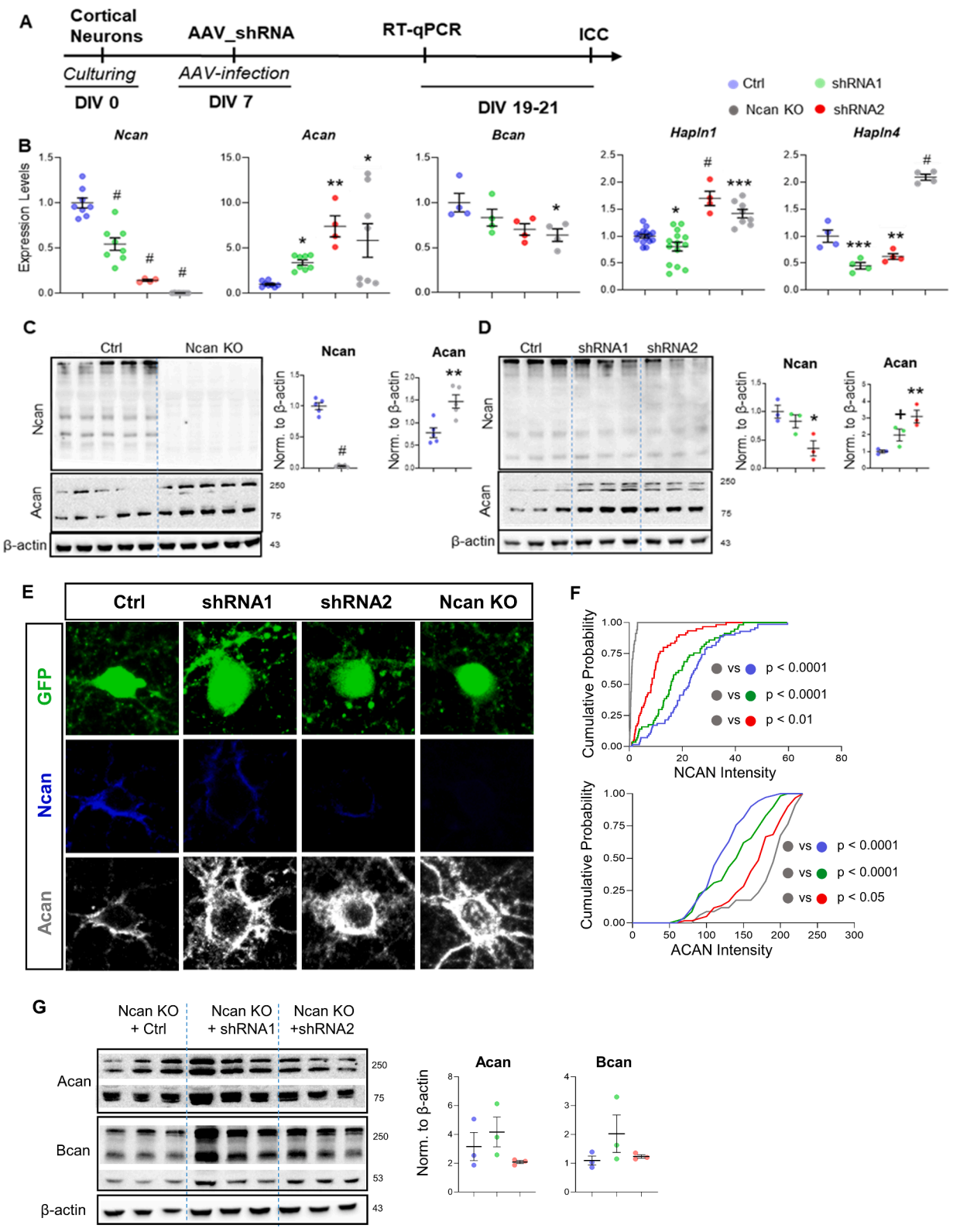

Fig. 1. Effect of Ncan depletion on expression of key ECM components.
(A) Timeline for *Ncan* knockdown experiments in primary cultured cortical cells. (B) qPCR analysis of ECM-associated gene products after Ncan depletion. (C, D) Western blot analysis of ECM proteins in *Ncan* KO and knocked down cortical cells, respectively. (E, F) Representative images of cortical cells infected with Ncan and control shRNA, expressing GFP, and associated analyses for Ncan and Acan intensities. The graphs show data from three independent experiments. One-way ANOVA with Sidak's comparisons and Kolmogorov-Smirnov's test were used for multiple comparison and the comparison of cumulative probability distributions, respectively. *$p < 0.05$, **$p < 0.01$, ***$p < 0.001$ and # $p < 0.0001$. (G) Quantification of protein levels of Acan and Bcan in KO cells infected with control, shRNA1 and shRNA2. The bar graphs show the mean ± SEM from three independent experiments. One-way ANOVA did not detect any treatment effects.

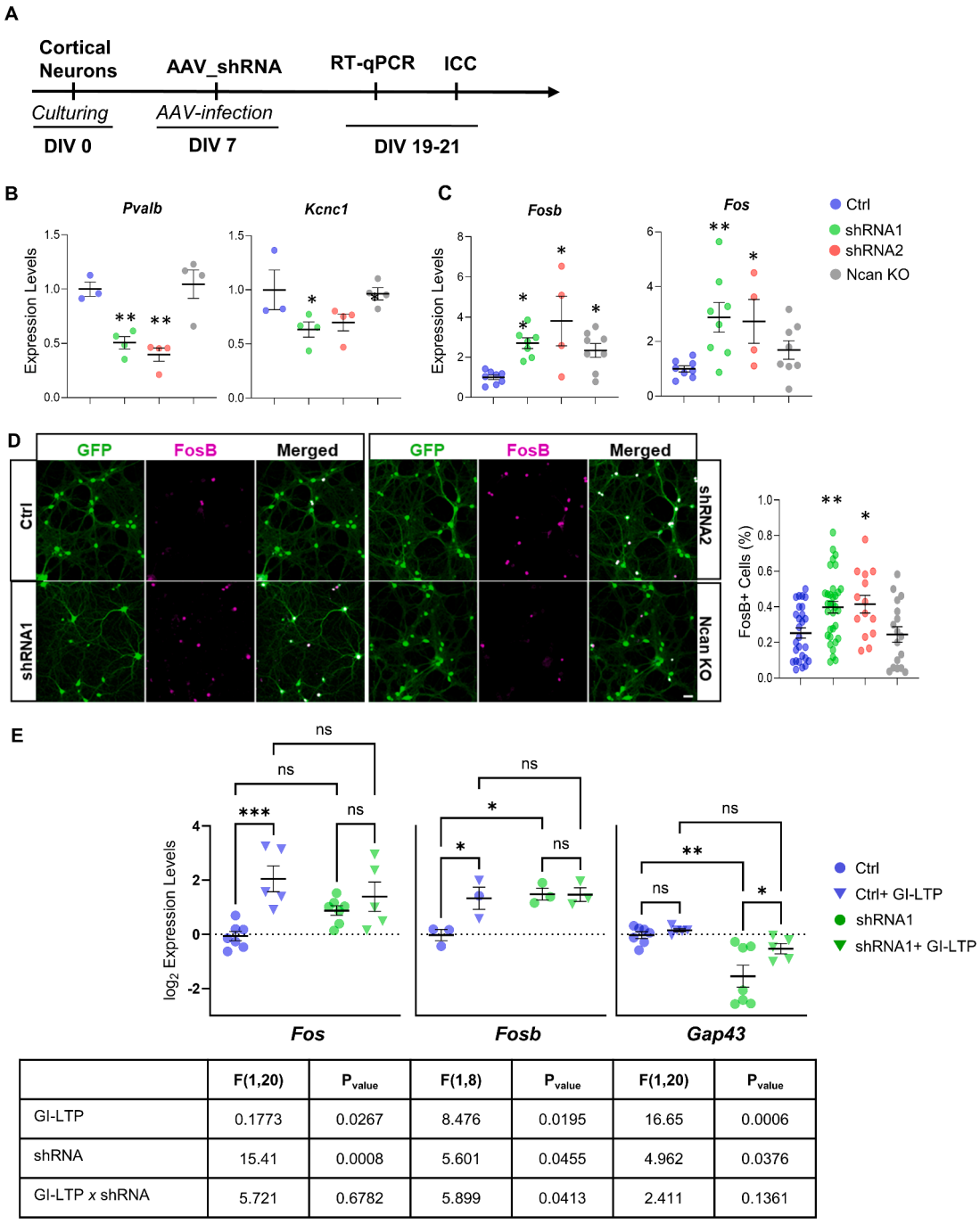

	F(1,20)	P_{value}	F(1,8)	P_{value}	F(1,20)	P_{value}
GI-LTP	0.1773	0.0267	8.476	0.0195	16.65	0.0006
shRNA	15.41	0.0008	5.601	0.0455	4.962	0.0376
GI-LTP *x* shRNA	5.721	0.6782	5.899	0.0413	2.411	0.1361

Fig. 2. The depletion of Ncan results in compromised expression of inhibitory neuron markers and cellular activity indicators *in vitro*.
(A) Timeline for the GI-LTP experiment in cortical cultures infected with control and shRNA1.
(B, C) qPCR evaluation of inhibitory markers (*Pvalb* and *Kcnc1*) and cellular activity markers (*Fos*b and *Fos*) after Ncan depletion. (D) Representative images of cortical cells infected with Ncan and control shRNA, expressing GFP, and associated analyses for the cell activity marker FosB. (E) qPCR evaluation of activity-associated genes *Fos, Fosb* and *Gap43* in the basal and GI-LTP conditions. The bar graphs show the mean ± SEM from three independent experiments. Table shows the results of two-way ANOVA. Holm-Šídák *post hoc* multiple comparisons test: $*p \leq 0.05$, $**p \leq 0.01$, and $***p \leq 0.001$.

activation of NMDA receptors (GI-LTP condition) (Fig. 2D). As anticipated, GI-LTP stimulation resulted in an elevation of mRNA levels of *Fos* and *Fosb* relative to baseline in Ctrl neurons. However, intriguingly, this effect was not observed in neurons after attenuation of Ncan expression (Fig. 2E), as there was a significant upregulation of the basal expression of *Fosb* and *Fos* in shRNA1-expressing relative to Ctrl neurons, indicating an overall increased activity level (Fig. 2C, E). Then, we investigated another synaptic plasticity-associated gene, the growth-associated protein 43 (GAP-43), which is involved in the presynaptic activity-dependent remodeling [43] and axonal regeneration [44]. Interestingly, *Gap43* was strongly downregulated in shRNA-infected cortical neurons under basal conditions compared to Ctrl. GI-LTP enhanced the expression of *Gap43* in shRNA conditions, but not to the Ctrl levels (Fig. 2E). These findings suggest the vital role of Ncan in regulation of neuronal activity and expression of plasticity-related genes.

Knockdown of Ncan expression enhanced the frequency of synaptic events and bursts in vitro

Thus far, we provided evidence for an overall increase in neuronal activity after Ncan depletion in cortical neurons. To further confirm the role of Ncan in regulating the balance between excitatory and inhibitory inputs, we conducted whole-cell patch clamp recordings in cortical neurons treated with Ctrl and shRNA AAVs and in *Ncan* KO neurons (Fig. 3A). Consistent with our expectations, we observed that Ncan depletion increased the synaptic inputs to cortical neurons infected with shRNA1 or shRNA2, and in *Ncan* KO neurons. In the Ncan shRNA1 or shRNA2-treated groups, all neurons displayed bursts of synaptic currents, whereas only 41.1 % and 62.2 % of the neurons in the Ctrl and *Ncan* KO exhibited such bursting phenotype (Fig. 3B,C). Further analysis demonstrated similar increases in the burst frequency, duration, and number of events in the shRNA1 group and *Ncan* KO and less prominent changes in shRNA2-expressing neurons (Fig. 3D).

Next, the recorded spontaneous events (postsynaptic currents) were categorized into two groups: burst-like events and events occurring between bursts (inter-burst events). Subsequently, we measured the frequency and amplitude of both types of events. Here, we compared burst features such as burst frequency, duration, and the number of events per burst, and found interesting patterns. Specifically, Ncan depletion was associated with a prominent increase in the frequency of spontaneous excitatory postsynaptic currents outside of bursts in shRNA-expressing and *Ncan* KO neurons as compared to Ctrl, indicating an elevated state of neuronal activity (Fig. 3E). The amplitude of currents was, on the other hand, comparable among all groups (Fig. 3G). The intraburst analysis demonstrated a notable and significant increase in the intraburst frequency of synaptic events in the shRNA2 and *Ncan* KO groups (Fig. 3F). shRNA1-infected neurons exhibited a frequency of sEPSCs similar to that observed in Ctrl neurons (Fig. 3G). Conversely, the amplitude of bursts was lower in shRNA2 and *Ncan* KO groups (Fig. 3H). Collectively, these findings strongly suggest that Ncan depletion contributes to the elevation of neuronal activity.

Knockdown of Ncan elevated AnkG expression at the AIS

Considering the accumulation of Ncan at the AIS, we further investigated the expression of AnkG, the major organizer of the AIS and regulator of neuronal excitability [20] in Ncan-depleted or -knockout cultures. We plotted AnkG intensity relative to the distance from soma and fitted a simple exponential model to estimate various parameters of AnkG distribution including maximum AnkG intensity (Y_{peak}), distance from the soma to the maximum intensity (X_{peak}), the distance at which maximum intensity reached 50 % (T_{decay}), and AnkG intensity at the proximal part of the AIS (Y0) (Fig. 4A–C). For each experimental group, the goodness of fit (R^2) exceeded the value of 0.9, indicating a high degree of model accuracy and that this model explains more than 90 % of the intra-group variance. Our observations indicate that depletion of Ncan by shRNA1 and shRNA2 altered the localization of AnkG within the AIS of cortical neurons, resulting in a displacement of the maximal AnkG expression distance from the soma, as compared to the Ctrl group. In contrast, the localization of AnkG in the *Ncan* KO neurons remained unaffected (Fig. 4C, D). The maximum intensity of AnkG, i.e., Y_{peak}, was found to increase in both shRNA1 and *Ncan* KO groups as compared to Ctrl, with no difference in shRNA2-expressing neurons (Fig. 4E). The distance at which AnkG expression reduces to 50 %, i.e., T_{decay}, showed significant differences between controls and all neurons with Ncan depletion or deletion, with shRNA1 and *Ncan* KO neurons showing similar values (Fig. 4F). No significant difference was observed in Y0 between the Ctrl and shRNA2 and shRNA1. In contrast, *Ncan* KO showed a significant difference compared to the Ctrl (Fig. 4G). Analysis of the relationships between each of AnkG-dependent parameters and electrophysiological features across experimental groups revealed that expression of AnkG at soma and the peak values are proportional to $\log_{10}$ (# of events) (Fig. 4H, I), the location of the AnkG peak is inversely related to the burst duration (Fig. 4 J), while T_{decay} is related to the frequency of events outside of the bursts (Fig. 4K).

Knockdown of Ncan expression reorganized AnkG distribution at the AIS of both inhibitory and excitatory neurons

Next, we assessed the impact of Ncan depletion on AnkG redistribution along the AIS of excitatory and inhibitory neurons separately. Here, we used GAD67 to identify GABAergic neurons in cutures (Fig. 5A, B). After observing inconsistent effects in cortical neurons infected with shRNA2, including extreme reduction of *Ncan* mRNA and upregulation of Bcan and Acan similar to shRNA1 and *Ncan* KO neurons, we decided to use shRNA1 for these experiments. It is possible that the contrasting effect on neuronal excitability in shRNA2 neurons was due to insufficient time for genetic compensation to occur [38].

Our results show that the Y_0 parameter, representing the AnkG intensity at the initial point of the AIS, is increased in Ncan shRNA1-expressing cells with no difference between GAD+ and GAD- neurons. The maximal intensity of AnkG was increased in GAD+ compared to GAD- neurons, and this effect appeared more prominent in Ncan shRNA1-expressing cells than in Ctrl (Fig. 5E). We noted an Ncan-independent proximal shift in the AnkG expression in the AISs of GAD+ inhibitory neurons in both Ctrl and Ncan shRNA1 conditions (Fig. 5F). Furthermore, the analysis revealed a reduction in T_{decay} in GAD+ relative to GAD- neurons within the Ctrl group (Fig. 5G). However, T_{decay} was increased by Ncan shRNA1 in GAD+ neurons, so no significant difference between GAD- and GAD+ cells was observed after the knockdown (Fig. 5G). Taken together, our findings reveal both general and neuron subtype-specific regulatory mechanisms of AIS organization driven by Ncan.

Knockdown of Ncan expression changes the expression of Na_v channels

Na_v channels and other components of AIS are known to be recruited to the AIS by the scaffold protein AnkG [11]. Vice versa, the knockdown of *Na_v* reduces the accumulation of AnkG [3]. Hence, we expected that the increase in AnkG may go hand-in-hand with increased expression of Na_v at the AIS. Immunoblot analysis showed no significant differences in the protein levels of $Na_v1.2$, $Na_v1.6$, and AnkG expression between Ctrl and *Ncan* KO neurons (Fig. 6A). However, there was a tendency for downregulation of $Na_v1.2$ by shRNA1 and a significant decrease of $Na_v1.2$ in shRNA2 neurons, as well as for upregulation in $Na_v1.6$ and AnkG expression in both shRNA groups (Fig. 6B). Western blot analysis of *Ncan* KO neurons treated with shRNA1 and shRNA2 revealed no significant difference in $Na_v1.6$ and AnkG protein levels, providing additional support to the specificity of the shRNA constructs used in this study (Fig. 6C).

Discussion

Our study demonstrates the importance of Ncan for the expression of key organizing proteins in the PNNs and AIS *in vitro*. It highlights Ncan's role in regulating neuronal activity with implications for synaptic plasticity.

Ncan knockdown and the PNN molecular organization

Ncan knockout and knockdown with two different shRNAs consistently resulted in elevated expression of Acan at the mRNA and protein levels globally and specifically in the PNNs. Acan, the primary and most abundant component of PNNs, is crucial in providing structural stability to these structures. In the absence or reduction of Ncan, the upregulation of Acan may serve as a compensatory response to maintain the structural integrity and functional properties of PNNs [45]. Interestingly, a previous study has demonstrated a strong correlation between neuronal

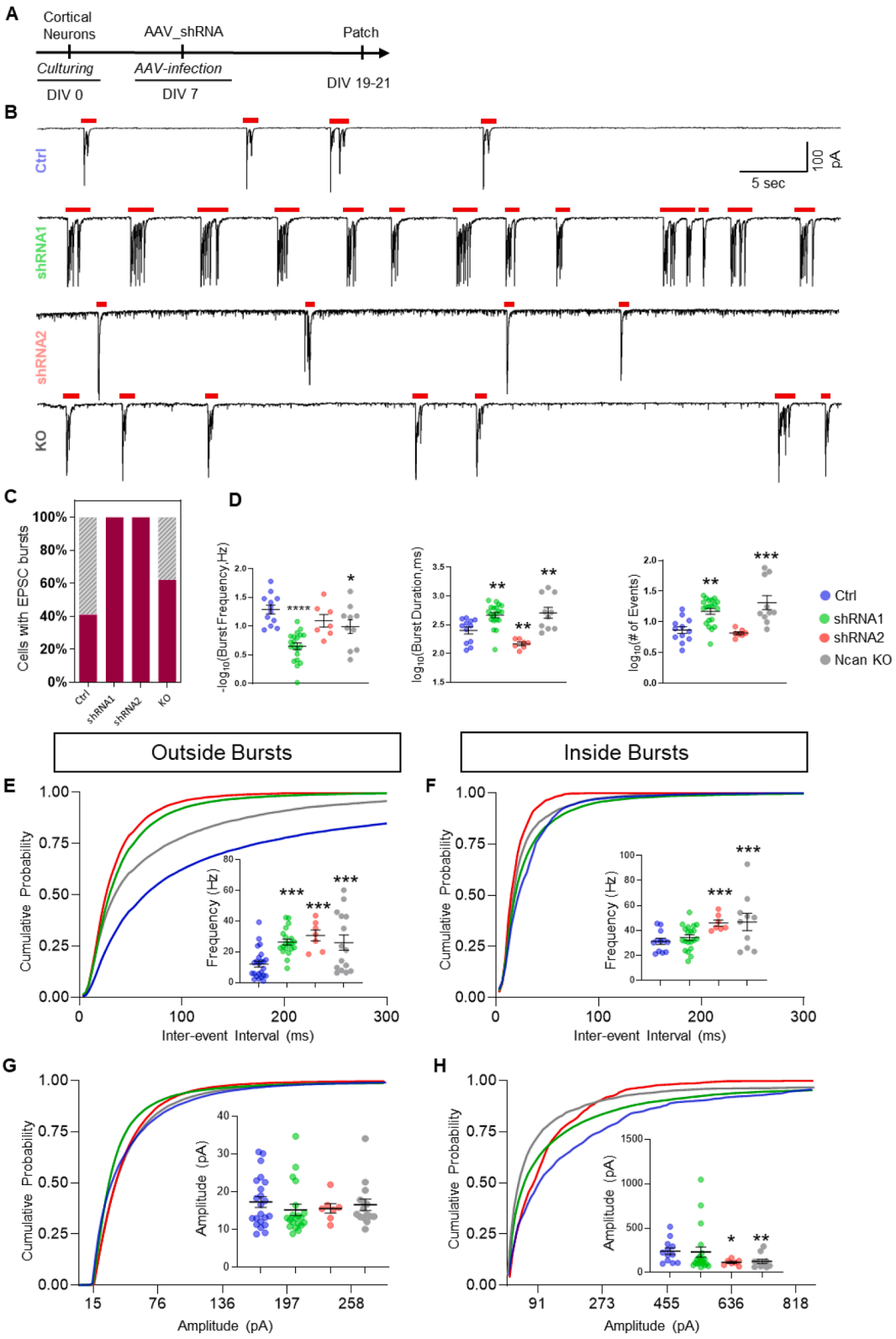

Fig. 3. The depletion of Ncan leads to enhanced sEPSCs and increased neuronal activity *in vitro*.
(A) Timeline of patch-clamp experiments for spontaneous EPSC recording in cultured cortical cells. (B) Representative traces of spontaneous EPSCs recorded at −70 mV in the cortical neurons infected with control and shRNAs. Red lines above the traces indicate areas considered as bursts, according to designed method for burst detection. (C) Quantification of the proportion of cells exhibiting burst activity across experimental groups. (D) Quantification of three distinct electrophysiological parameters, burst frequency, burst duration, and number of spikes per burst, across multiple experimental groups. (E, F) Cumulative probability curves for inter-event intervals and calculated frequency of EPSCs occurring within and outside of bursts. (G, H) Cumulative probability analysis of the amplitude of EPSCs occurring within and outside of bursts. The bar graphs show the mean ± SEM from three independent experiments. One-way ANOVA with Sidak's comparisons were used for multiple comparison. *$p < 0.05$, **$p < 0.01$, ***$p < 0.001$ and **** $p < 0.0001$.

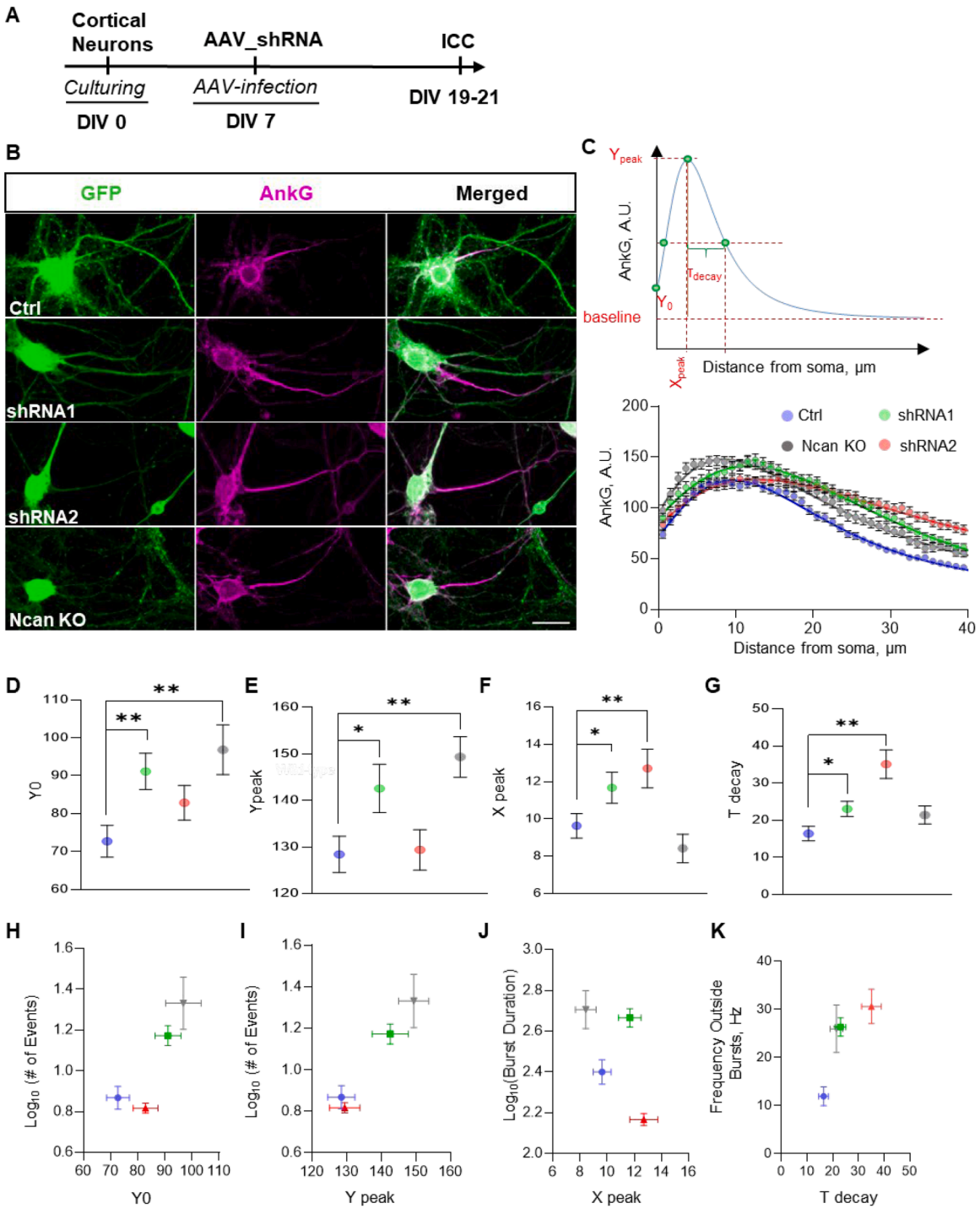

Fig. 4. Ncan depletion alters AnkG distribution along the AIS.
(A) Experimental timeline. (B) Representative images of cortical neurons infected with Ncan and control shRNA, expressing GFP, immunostained for AnkG. (C) Model depicting the quantification of various parameters related to AnkG expression, alongside the fitted model correlating with observed events. (D–G) Quantification of AnkG-associated parameters, including Y0 (the amount of ankG at the proximal part of the axon), Y_{peak} (the peak height), X_{peak} (distance from the soma to the maximum intensity), and T_{decay} (the distance at which maximum intensity reached 50 %), across experimental groups. (H–K) Correlation of various AnkG-dependent parameters with electrophysiological features across experimental groups. The bar graphs show the mean ± SEM three independent experiments. Statistical significance for panels D–G was calculated via bootstrap approach as described in Materials and Methods. *$p < 0.05$, and **$p < 0.01$.

activity and *Acan* levels [46] after treating cortical neurons with bicuculline, an inhibitor of $GABA_A$ receptors [47,48], thereby increasing the excitability of excitatory neurons. The increased neuronal activity upregulated c-Fos and Acan levels, and their expression returned to control levels once silenced with tetrodotoxin treatment [46]. Similarly, we show that Ncan depletion upregulates neuronal activity, Acan and c-Fos levels. This finding, therefore, implies that the increase in Acan levels might be a consequence of elevated activity in Ncan-depleted cultures, which may represent a homeostatic protective response as it has been shown that PNNs support perisomatic inhibition and offer protective properties to fast-spiking interneurons [49], and Acan as a central element in PNN formation [40,50]. As Acan is the major carrier

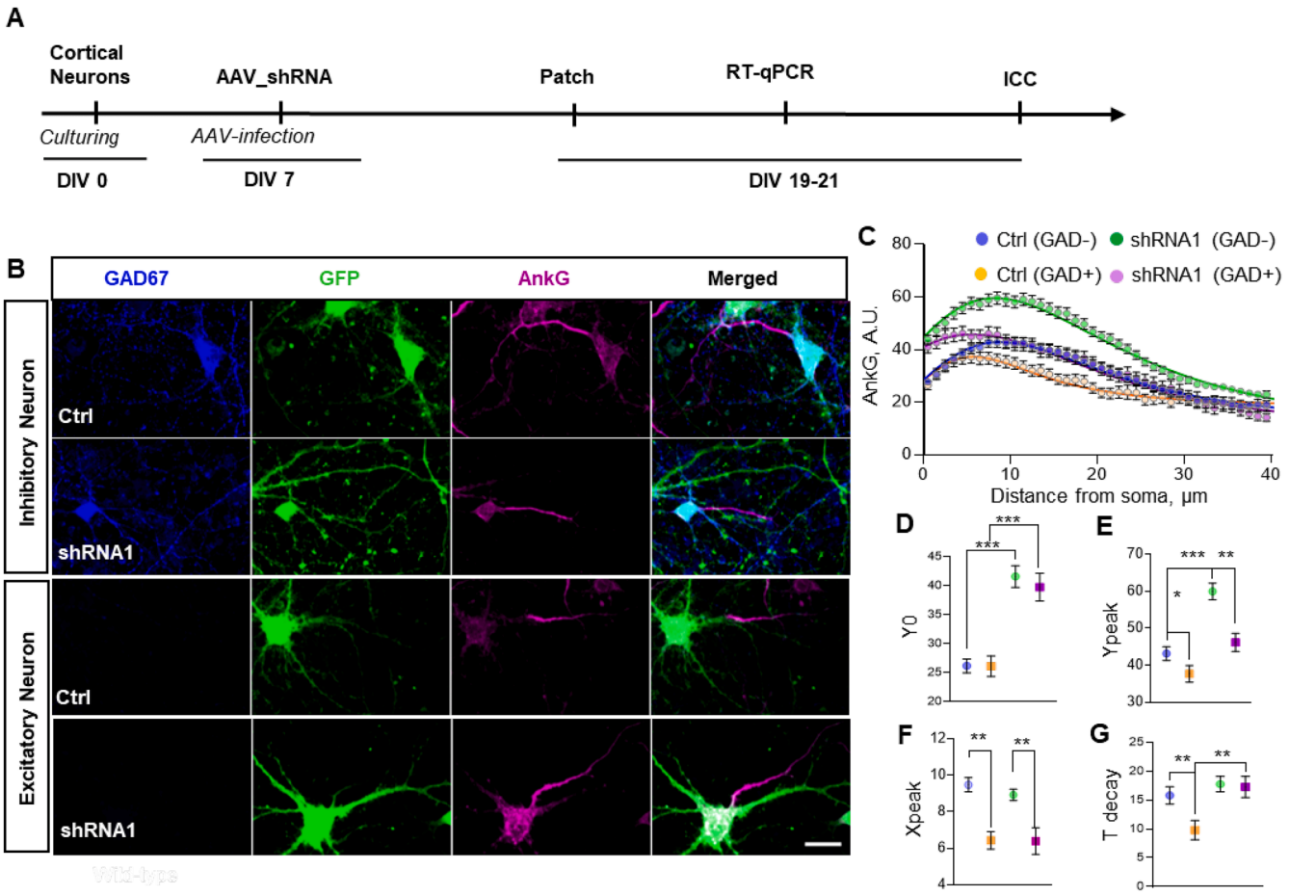

Fig. 5. The depletion of Ncan alters AnkG parameters in excitatory and inhibitory neurons.
(A) Experimental timeline. (B) Representative images of cortical neurons infected with Ncan and control shRNA, expressing GFP and immunostained for AnkG and the inhibitory neuron marker GAD67. (C) Graph depicting the fitted model correlating with observed AnkG expression in GAD67 positive and negative cells across experimental groups. (D–G) AnkG-dependent parameters in GAD67-positive and GAD67-negative neurons within control and shRNA1 experimental groups. The bar graphs show the mean ± SEM from three independent experiments. Statistical significance for panels D-G was calculated via bootstrap approach as described in Materials and Methods. $^{**}p < 0.01$, and $^{***}p < 0.001$.

of *Wisteria floribunda* agglutinin (WFA)-binding glycoepitopes *in vitro* [40], it is plausible to assume that the increase in Acan is accompanied by the increase in WFA in our conditions.

For other ECM molecules, more complex dependencies on Ncan were revealed. The level of *Hapln1* mRNA was reduced by weak *Ncan* knockdown with shRNA1 and increased by more potent knockdown with shRNA2 and by *Ncan* knockout. Both Ncan shRNAs decreased *Hapln4* mRNA, while *Ncan* knockout increased it. Thus, both *Hapln1* and *Hapln4* expression seem to follow a U-shaped expression pattern in relation to Ncan availability. These data show that Ncan regulates the expression of Acan and link proteins as key organizers of PNNs, and that *Ncan* knockout results in some compensatory effects not observed after knockdown of *Ncan*. It is important to mention that the density of glial cells is rather low in dissociated cortical cultures employed in the present work, which allowed us to focus primarily on the role of neuronal Ncan. This can be viewed as both an advantage and a limitation of the experimental model used.

Ncan depletion increases neuronal activity

Ncan has been demonstrated to be crucial for the development of neuronal circuits and is known to be involved in controlling synaptic plasticity [51,52]. Here, we found that *Ncan* knockdown resulted in an upregulation in activity-dependent gene expression of c-Fos and FosB, an increase in the number of c-Fos-immunopositive cells, and prominent enhancement in neuronal activity within and between bursts in cultured cortical neurons. One of underlying mechanisms seems to be mediated by the reduction in expression of Pvalb and of Kcnc1, the potassium channels important for fast-spiking of Pvalb-positive neurons. Previous studies have reported similar changes after PNN degradation by chondroitinase ABC [46]. The amount of parvalbumin in Pvalb-positive interneurons increases with their maturation [53] and has been shown to affect the acquisition of their mature phenotypes [54]. A critical role for the ECM in modulating neuronal firing activity and maintaining the delicate balance between excitation and inhibition has been well documented in previous studies [22,23,55,56]. Earlier findings suggested that the ECM aids in preserving the balance between excitatory and inhibitory neurons by upholding inhibitory connections [57,58]. Consequently, removing ECM resulted in a significant decrease in inhibitory synapse density [59]. A recent investigation proposed that astrocyte-secreted Ncan is critical in preserving the integrity of inhibitory synapses. Noteworthy, *Ncan* deletion reduced the frequency of miniature inhibitory postsynaptic currents in cortical neurons of *Ncan* KO mice [60]. Thus, increased excitation under conditions of Ncan deficiency is likely to reflect an interplay of multiple factors, such as the loss of inhibitory synapses, abnormal PNNs, reduced Kcnc1 expression in Pvalb-positive interneurons, and AIS remodeling.

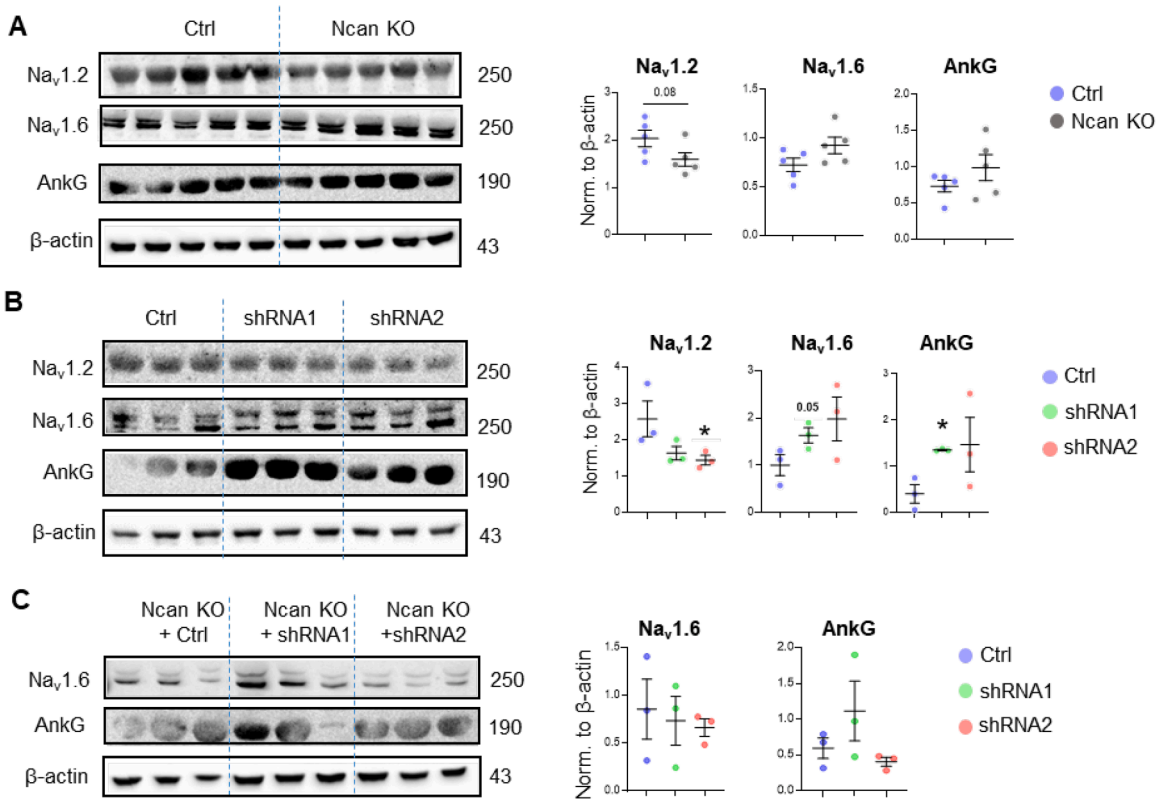

Fig. 6. The depletion of Ncan changes the protein levels of sodium channels and AnkG.
(A) Western blot analysis of $Na_v1.2$, $Na_v1.6$, AnkG, and β-actin from the cell lysates of wild-type and KO samples. (B) Western blot analysis of $Na_v1.2$, $Na_v1.6$, AnkG, and β-actin in cell lysates from control, shRNA1- and shRNA2-infected cultures. (C) Quantification of protein levels of $Na_v1.6$ and AnkG in KO cells infected with control, shRNA1 and shRNA2. The bar graphs show the mean ± SEM from three independent experiments. One-way ANOVA with Sidak's multiple comparisons test. $^*p \leq 0.05$.

Ncan knockdown and AIS remodeling

The precise positioning and composition of the AIS at the proximal axon play a critical role in determining the excitability of neurons [1]. Here, we observed a distal shift in the peak of AnkG localization following Ncan depletion in shRNA-infected neurons and elevated profile of AnkG expression in *Ncan* KO neurons. The shift correlated with increased neuronal excitability. This finding aligns with a theoretical analysis that emphasizes the increase in neuronal excitability due to a distal shift in the AIS in the absence of hyperpolarizing currents [61]. AIS exhibits a high concentration of voltage-gated ion channels, particularly sodium channels. Interestingly, in line with our observation of reduced $Na_v1.2$ concentration after Ncan depletion, Zhang and colleagues showed that deficiency in $Na_v1.2$ channels induces neuronal hyperexcitability in adult mice [62]. The result provides a potential explanation for the clinical observation that individuals with $Na_v1.2$ deficiency experience seizure activity [63]. Alterations in the expression and functionality of $Na_v1.6$ channels have a significant impact on the firing properties of neurons [64], and effective elimination of action potential propagation has been observed in *$Na_v1.6$* KO mice [65], as well as after $Na_v1.6$ pharmacological inhibition [66]. A comparable pattern of neuronal activity was observed in our experiments when Ncan depletion resulted in the upregulation of $Na_v1.6$ at the protein level, leading to neuronal hyperexcitability. Although the exact role of Ncan in redistribution of AnkG is unclear at this stage, it is in line with previous studies that suggested a role of the ECM in the organization and functionality of the AIS via interactions with NF186 and sodium channels [11,67,68].

Ncan knockdown and synaptic plasticity

To further study the effects of Ncan downregulation on synaptic plasticity, we searched for expression changes of activity-related genes after induction of chemical LTP. One major finding is the reduced expression of *Gap43* in both basal and GI-LTP conditions. Previous studies have shown a strong relationship between *Gap43* expression and memory. For example, overexpression of *Gap43*, as seen in the hippocampus of Alzheimer's patients, impaired learning and memory whereas moderate expression improved it [69,70]. Also a reduced expression of *Gap43* as found here resulted in memory dysfunction [70]. On the other hand, the enhanced basal expression of FosB observed after *Ncan* knockdown in cortical neurons is also an interesting finding as its expression strongly correlates with neural epileptiform activity [71]. In AD patients and several AD animal models, subclinical epileptiform activity has been reported, which correlates strongly with the chronic accumulation of *FosB*, impacting also the expression of *Fos* [72,73]. Interestingly, overexpression of *FosB* is also shown to impact hippocampal learning and memory, possibly through *FosB*-dependent induction of immature spines [74]. Moreover, the acute neuronal activity-dependent upregulation of *Fos* that is essential for LTP-dependent synaptic plasticity [75], i.e. the cellular and molecular form of learning and memory, did not occur in cortical cells after *Ncan* knockdown. This is in agreement with a previous work in which basal *Fos* expression was found to be upregulated in memory-impaired aged mice [76].

Potential relation to human neuropsychiatric disorders

Genome-wide association studies (GWAS) have previously identified a polymorphism in the human *NCAN* gene, rs1064395, in the risk for bipolar disorder [27], and for schizophrenia [77]. *Post mortem* eQTL analyses have suggested that the *NCAN* polymorphism might be associated with slightly increased levels of *NCAN* and the neighboring gene product *HAPLN4* in the dorsolateral PFC [33], while the association of the risk variant with the manic phenotype resembles the behavioral phenotype of *Ncan*-deficient mice [28], pointing to a potentially detrimental effect of both increased as well as decreased Ncan levels. Gene expression analysis across brain regions revealed widespread upregulation of *ACAN, BCAN, NCAN* and neuroglycan-C in schizophrenia patients and increased *NCAN* expression was associated with greater cognitive impairment [78]. Upregulation in expression of ECM genes but impaired expression of PNNs in schizophrenia patients and mouse models can be explained by activation of glial cells and elevated turnover/proteolysis of ECM proteoglycans [79–81]. Our present findings have revealed a regulatory role for NCAN in the expression and cellular distribution of AnkG. The *ANK3* gene, which encodes the human AnkG protein, has also been identified in GWAS of schizophrenia and bipolar disorder [82,83]. Notably, expression studies suggest an increased expression of *ANK3* in both disorders [84], mirroring the increased AnkG expression upon *Ncan* depletion observed here. More broadly, our results suggest that reduced *Ncan* expression might contribute to an altered excitation-inhibition ratio hypothesized to be a key circuit mechanism in the major psychoses [85], which, at a systems level, may be reflected by a manic phenotype [28] and tonically increased hippocampal activity [33,86].

In conclusion, our study highlights the importance of Ncan in regulating the expression patterns of Acan, Bcan, Pvalb, Kcnc1, AnkG and $Na_v1.6$, neuronal activity and synaptic plasticity-related genes in cortical neurons. Our results point to a complex regulatory role of Ncan in the regulation of multiple proteins implicated in neuropsychiatric disorders like bipolar disorder and schizophrenia, thereby shedding new light on the previously reported genetic association of the human NCAN gene with these disorders.

Experimental procedures

Knockdown experiments using Ncan shRNA

To knock down mouse Ncan (GeneID: NM_007789.3), shRNA plasmids were cloned by the insertion of the siRNA sequences (Sigma) shown to be effective against Ncan mRNA [87,88] (Suppl. Table 1) targeting the open reading frame into AAV U6 GFP (Cell Biolabs Inc., San Diego, CA, USA) using BamH1 (New England Biolabs, Frankfurt a. M., Germany) and EcoR1 (New England Biolabs, Frankfurt a.M., Germany) restriction sites. Two shRNAs were produced targeting Ncan messenger RNA (mRNA) (Ncan shRNA) by selecting target sequences in the coding regions of Ncan to prevent or minimize off-target effects [89]. The shRNA universal negative control (Sigma, Control shRNA) was used as a non-targeting control (Suppl. Table 1). Positive clones were sequenced and used for the production of recombinant adeno-associated viral particles as described previously [90]. HEK 293T cells were transfected using PEI (1ng/µl) with an equimolar mixture of the shRNA encoding AAV U6 GFP, pHelper (Cell Biolabs Inc., San Diego, CA, USA), and RapCap DJ plasmids (Cell Biolabs Inc., San Diego, CA, USA). From 48 to 72 h after transfection, freeze-thaw cycles were implemented to lyse cells and then treated with benzonase (50 U/mL; Merck Millipore, Burlington, MA, USA) for 1 h at 37 °C. Lysates were centrifuged at 8000 × g at 4 °C, supernatants collected, and filtered with a 0.2-µm filter. We then purified filtrates using the pre-equilibrated HiTrap Heparin HP affinity columns (GE HealthCare, Chicago, IL, USA), followed by washing with the following buffers in sequence; Wash Buffer 1 (20 mM Tris, 100 mM NaCl, pH 8.0; sterile filtered) and wash buffer 52 (20 mM Tris, 250 mM NaCl, pH 8.0; sterile filtered). Elution buffer (20 mM Tris, 500 mM NaCl, pH 8.0; sterile filtered) was then used to elute viral particles. Finally, Amicon Ultra-4 centrifugal filters with 100 kDa molecular weight cutoff (Merck Millipore, Burlington, MA, USA) along with 0.22 µM Nalgene® syringe filter units (sterile, PSE, Sigma-Aldrich, St. Louis, MO, USA) were used to further purify viral particles before being aliquoted and stored at -80°C.

Cell culture, neuronal infection, RT-qPCR, and GI-LTP

Cortical neurons were isolated from embryonic (E18) C57BL6/J mice or *Ncan* KO mice [51], as described previously [91]. After harvesting, neurons were plated on poly-l-lysine-coated (Sigma; Cat. No. 2636) 6 well plates without coverslips at a cell density of 500,000 neurons per well. Neurons were maintained in 2.5 ml of Neurobasal media (Invitrogen) supplemented with 2 % B27 and 1 % L-glutamine and 1 % Pen-Strep (Life Technologies). Dissociated wildtype and *Ncan* KO cortical neurons were initially infected with Control and the two Ncan shRNA AAVs at 7 days *in vitro* (DIV) and mRNA expression levels of *Ncan* were assayed at DIV 21. Knockdown efficiencies of the two Ncan shRNAs normalized to the Control shRNA were determined using RT-qPCR. From cortical cultures, total RNA was extracted using the EURx GeneMatrix DNA/RNA Extracol kit (Roboklon, Cat. No. E3750) according to the manufacturer's recommendations [92] and products were further checked for genomic DNA contamination by using NanoDrop™ 2000c spectrophotometer (ThermoFisher) and gel electrophoresis to measure the RNA yield, purity, and integrity, respectively. Then, 2 µg of RNA was used for cDNA conversion using the High-Capacity cDNA Reverse Transcription Kit (ThermoFisher Scientific, Cat. No. 4368814). qPCR analysis was performed with TaqMan™ gene expression array assay (ThermoFisher Scientific, Cat. No. 4331182) using the Quant-Studio-5 (Applied Biosystems). Details of all TaqMan™ probes used are given in (Suppl. Table 2). Finally, gene expression per sample was normalized relative to the expression of glyceraldehyde 3-phosphate dehydrogenase (*Gapdh*) [93]. For the glycine-induced form of chemical LTP (GI-LTP), already shRNA1 AAV infected cortical cultures were first incubated with sterile artificial cerebrospinal fluid (ACSF) containing the following (in mM): 119.0 NaCl, 1.3 $MgSO_4$ 1.0 NaH_2PO_4, 26.2 $NaHCO_3$, 2.5 KCl, 2.5 $CaCl_2$, 11.0 glucose, 0.2 glycine, for 5 min at 37°C before returning to ACSF without glycine for 50 min [94], whereas control cultures were incubated in ACSF.

Immunocytochemistry (ICC)

Cortical neurons from wildtype and *Ncan* KO mice from DIV 21–23 were used for immunocytochemistry experiments. Neurons were washed and fixed with phosphate-buffered saline (PBS) and 4 % paraformaldehyde (PFA) for 10 min, respectively. They were then permeabilized with 0.1 % Triton X-100 in PBS for 10 min, washed 3 times, and blocked (0.1 % Glycine + 0.1 % Tween-20 + 10 % Normal Goat Serum in PBS) for 60 min at room temperature. Then, the neurons were labeled with primary and secondary antibodies (Suppl. Tables 3 and 4, respectively), and finally mounted (Fluoromount; Sigma Aldrich, F4680–25ML) for imaging.

Imaging and data acquisition

Next, the mounted coverslips were imaged using a Zeiss LSM 700 confocal microscope. Z-stacked images of neurons were randomly obtained across the entire surface of the coverslips, barring the edges, using a 63x/1.4 NA oil immersion objective. Throughout all the imaging sessions, we maintained the acquiring conditions to compare fluorescence intensity between groups. For analysis of AnkG images, we used the previously described procedure [24]. Here, using GFP signal to identify shRNA infected neurons and the AnkG immunolabeling, the AISs were first manually outlined and analyzed from the soma edge over a 40 µm

long distance with a line profile (width=3.0) with Fiji [24]. For the quantification of ECM molecules in shRNA-treated cortical neurons, we automatically outlined the profile of the cell somata of GFP+ and Acan+ neurons and created a band of 1.5 μm as the region of interest (ROI). Additionally, for FosB images, we used GFP+ neurons to automatically select soma of neurons, then we masked and overlayed the masks over FosB original images to measure fluorescent intensity as well as percentage density.

Further processing of AnkG data

The experimentally obtained distribution of AnkG along the length of the axon was binned with a one-micron step size. The resulting data were averaged for each group under investigation. The resulting curve was fitted with the sum of two exponentials with weights a1 and a2 plus a baseline (b):

$$AnkG = a1*e^{-\frac{x}{t1}} + a2*e^{-\frac{x}{t2}} + b$$

Subsequently, numerical values were obtained for each fitted curve: the amount of AnkG at the beginning of the axon (Y0), the peak height (Y peak) and position (X peak), as well as the distance from the peak where the AnkG amount decreased by a factor of two (T_{decay}).

To estimate the confidence intervals of the parameters, bootstrap resampling was employed. Specifically, for each group under investigation, a sample of axons corresponding to that group was randomly selected with replacement. The described parameters were then computed based on the resampled data. This procedure was repeated 10^4 times, and the standard deviations of the resulting distributions were represented on the figures as error bars.

Statistical significance of pairwise comparisons was assessed using shuffling. In detail, when comparing two groups, a subset of experimental data containing axons exclusively from one of the groups was extracted. The axon's group membership was then randomly assigned, and the data were averaged to compute the parameters of the AnkG distribution along the axon for each of the two pseudogroups. After 10^4 repetitions, the null distribution for each parameter was obtained as the difference between the distributions for each group. The p-value was calculated as the quantile corresponding to the observed difference between the parameters.

SDS-PAGE and Western blotting

The GeneMATRIX DNA/RNA/Protein Purification Kit (EURX Cat. No. E3597) was used to purify total protein from cortical cells. The concentration of the resulting protein pellet was determined using the Pierce™ BCA Protein Assay Kit (ThermoFisher Cat. 23225) and a NanoDrop™ 2000c spectrophotometer (ThermoFisher). The protein samples were boiled for 5 min at 95 °C and 10 μg were loaded onto each lane of a 10 % SDS gel. Electrophoresis was carried out for 2 h at 90 V in a tank containing cold 1X TGS (Tris/Glycine/SDS) buffer. The separated proteins were transferred onto nitrocellulose membranes using the Trans-Blot Turbo transfer system (Bio-Rad). To block nonspecific binding, a tris-buffered saline solution with 0.1 % Tween 20 (TBST) supplemented with 5 % skim milk (SERVA, Cat. 42590.01) was used for 1 h at room temperature. The primary antibodies were diluted in TBST/1 % milk and applied to the membranes overnight on a shaker at 4 °C. The blots were washed three times for 10 min with TBST and incubated for one hour with Horseradish Peroxidase (HRP)-conjugated secondary antibodies diluted at 1/10,000. After three washes in TBST, the blots were developed using the SuperSignal® West Pico Chemiluminescent Substrate (ThermoScientific Cat. 34078). The membranes were incubated with a working solution containing peroxide solution and luminol enhancer at a 1:1 ratio for 5 min at room temperature. The excess reagent was removed and the blots were imaged using a chemiluminescence Imager (Azure Biosystems C300) and covered with clear plastic wrap.

Whole-cell patch-clamp recording

Recording spontaneous excitatory postsynaptic currents (sEPSCs) allows for the estimation of overall neuronal activity in the absence of stimulation when the membrane potential is held at resting potential (-70 mV) using voltage-clamp technique**.** Whole-cell patch clamp recordings were performed as described previously [95]. Briefly, coverslips containing cortical cells were immediately transferred from culture media to the submerged recording chamber and immersed in pre-warmed recording solution containing (in mM): 105 NaCl, 3 KCl, 10 HEPES, 5 Glucose, 2 $CaCl_2$, and 1 $MgCl_2$. Large cells with a pyramidal shape (presumably excitatory neurons) were selected for recordings under visual control using infrared differential interference contrast optics (Slicescope, Scientifica, UK) and 40X water immersion objective on the SliceScope Pro 6000 upright fixed-stage microscope (Scientifica) and a patch-clamp EPC10 amplifier (HEKA, Lambrecht, Germany). The patch pipettes were pulled from borosilicate glass capillary (wall thickness 0.315 mm, length 100 mm, outer diameter 1.5 mm, Hilgenberg) using a DMZ universal electrode puller (Zeitz Instruments GmbH, Martinsried, Germany) and filled with intracellular solution containing (in mM): 90 KCl, 3 NaCl, 5 EGTA, 5 HEPES, 5 Glucose, 0.5 $CaCl_2$, and 4 $MgCl_2$. A 3–5 MΩ resistance has been achieved when the pipets are filled with intracellular solution. The whole-cell configuration was obtained by providing a brief suction after establishing a MΩ seal. Only recordings were approved if the series resistance was less than 20 MΩ and did not fluctuate by more than 20 % during the experiment. The holding potential was adjusted to -70 mV and the recordings were filtered at 10 kHz and sampled at 20 kHz. Properties of sEPSC were calculated by MiniAnalysis (Synaptosoft Inc., USA) using detection parameters of 5 pA for event threshold. To analyze the characteristics of neuronal activity, we developed a method to detect bursts in sEPSC recordings. First, the moving median absolute deviation of the sEPSC signal using a 100 ms window was calculated and the resulting curve was binarized using a threshold of 20 pA and applied a median filter with a 100 ms window to smooth the signal. Any periods below the binarized signal were considered as no-burst intervals. We then excluded non-burst intervals shorter than 0.2 s and identified the start and stop times of the remaining non-burst intervals. To further refine our burst analysis, we excluded any bursts that were shorter than 0.1 s and had a maximal or average amplitude below 250 pA and 50 pA, respectively.

To avoid contamination of non-burst intervals by bursts, we defined a "protection" zone around each burst as a time window that extended 50 ms before and 200 ms after the burst. Events within this time window were considered "protected" events and were excluded from the analysis. The final output of our method was a classification of each time point in the original sEPSC signal. Time points within bursts were classified as "bursty", time points within the protection zone were classified as "protected", and time points outside of bursts and the protection zone were classified as "nonbursty". Protected events were excluded from the analysis to ensure that non-burst intervals were not contaminated by bursts. The burst detection script is available at https://github.com/dityatev-lab/burst_detection.

Statistical analysis

Statistical analysis was performed using GraphPad Prism 8.0 (GraphPad Software Inc., La Jolla, USA) and Statistica 8.0 (StatSoft, USA) software. All data are shown as mean ± SEM with n being the number of mice. Asterisks in figures indicate statistical significance (with details in the figure legend or Results). The hypothesis that experimental distributions follow the Gaussian law was verified using Kolmogorov-Smirnov, Shapiro-Wilk, or D'Agostinio tests. For pairwise comparisons, we performed the Students' *t*-test where the samples qualify for the normality test; otherwise, the Mann-Whitney test was

employed. Additionally, Wilcoxon matched-pairs test was used for paired data that did not pass the normality test. Holm-Sidak's multiple comparisons *t*-test was used for independent comparisons. Spearman correlation coefficients were computed to estimate the correlation between the variables studied. As indicated, one and two-way ANOVA with uncorrected Fisher's LSD as well as Brown-Forsythe with Welch ANOVA tests, were also used. The p-values represent the level of significance as indicated in figures by asterisks (*$p < 0.05$, **$p < 0.01$, ***$p < 0.001$ and **** $p < 0.0001$).

Abbreviations

Acan, aggrecan; ACSF, artificial cerebrospinal fluid; AIS, axon initial segment; AnkG, ankyrin G; AP, action potential; Bcan, brevican; CNS, central nervous system; Ctrl, control; ECM, extracellular matrix; HAPLN1, hyaluronan and proteoglycan link protein 1; HRP, horseradish peroxidase; GAP-43, growth-associated protein 43; GAPDH, glyceraldehyde 3-phosphate dehydrogenase; ICC, immunocytochemistry; Kcnc1, Potassium voltage-gated channel subfamily C member 1; KO, knockout; Na_v, voltage-gated sodium channel; Ncan, neurocan; PAF, paraformaldehyde; PNN, perineuronal net; Pvalb, parvalbumin; ROI, region of interest; sEPSCs, spontaneous excitatory postsynaptic currents; TBST, tris-buffered saline solution with 0.1 % Tween 20; T_{decay}, distance at which intensity reached 50 % of maximal intensity; TnR, tenascin-R; Vcan, versican; WFA, *Wisteria floribunda* agglutinin; X_{peak}, distance from the soma to the maximum intensity; Y0, intensity at the proximal part of the AIS; Y_{peak}, maximal intensity

Funding

This work has been supported by DAAD (fellowship to David Baidoe-Ansah), Deutsche Forschungsgemeinschaft (DFG, German Research Foundation) – Project-ID 425899996 – SFB 1436 (to Alexander Dityatev, Björn H Schott and Constanze Seidenbecher) and Project-ID 362321501 - RTG 2413 SynAge (to Alexander Dityatev and Constanze Seidenbecher).

Ethical approval

Animal handling for isolation of cortical neurons from embryonic mice followed the ethical guidelines of Directive 2010/63/EU, German law, and Saxony-Anhalt state's Ethical Committee on Animal Health and Care.

Consent for publication

All authors have approved the last version of this manuscript for publication.

Declaration of competing interest

The authors declare no competing interests.

Acknowledgments

We thank Katrin Böhm and Jenny Schneeberg for technical support.

Supplementary materials

Supplementary material associated with this article can be found, in the online version, at doi:10.1016/j.matbio.2025.01.001.

Data availability

Data will be made available on request.

References

[1] C.Y. Huang, M.N. Rasband, Axon initial segments: structure, function, and disease, Ann. N. Y. Acad. Sci. 1420 (1) (2018) 46–61.
[2] T. Torii, Y. Ogawa, C.H. Liu, T.S. Ho, H. Hamdan, C.C. Wang, J.A. Oses-Prieto, A. L. Burlingame, M.N. Rasband, NuMA1 promotes axon initial segment assembly through inhibition of endocytosis, J. Cell Biol. 219 (2) (2020).
[3] C. Leterrier, N. Clerc, F. Rueda-Boroni, A. Montersino, B. Dargent, F. Castets, Ankyrin G membrane partners drive the establishment and maintenance of the axon initial segment, Front. Cell Neurosci. 11 (2017) 6.
[4] A. Lorincz, Z. Nusser, Molecular identity of dendritic voltage-gated sodium channels, Science 328 (5980) (2010) 906–909 (1979).
[5] A. Battefeld, B.T. Tran, J. Gavrilis, E.C. Cooper, M.H. Kole, Heteromeric Kv7.2/7.3 channels differentially regulate action potential initiation and conduction in neocortical myelinated axons, J. Neurosci. 34 (10) (2014) 3719–3732.
[6] A.Y. Lopez, X. Wang, M. Xu, A. Maheshwari, D. Curry, S. Lam, A.M. Adesina, J. L. Noebels, Q.Q. Sun, E.C. Cooper, Ankyrin-G isoform imbalance and interneuronopathy link epilepsy and bipolar disorder, Mol. Psychiatry 22 (10) (2017) 1464–1472.
[7] S.A. Freeman, A. Desmazieres, D. Fricker, C. Lubetzki, N. Sol-Foulon, Mechanisms of sodium channel clustering and its influence on axonal impulse conduction, Cell Mol. Life Sci. 73 (4) (2016) 723–735.
[8] J. Wang, S.W. Ou, Y.J. Wang, Distribution and function of voltage-gated sodium channels in the nervous system, Channels 11 (6) (2017) 534–554 (Austin).
[9] M.R. Kaplan, A. Meyer-Franke, S. Lambert, V. Bennett, I.D. Duncan, S.R. Levinson, B.A. Barres, Induction of sodium channel clustering by oligodendrocytes, Nature 386 (6626) (1997) 724–728.
[10] A. Brachet, C. Leterrier, M. Irondelle, M.P. Fache, V. Racine, J.B. Sibarita, D. Choquet, B. Dargent, Ankyrin G restricts ion channel diffusion at the axonal initial segment before the establishment of the diffusion barrier, J. Cell Biol. 191 (2) (2010) 383–395.
[11] K.L. Hedstrom, X. Xu, Y. Ogawa, R. Frischknecht, C.I. Seidenbecher, P. Shrager, M. N. Rasband, Neurofascin assembles a specialized extracellular matrix at the axon initial segment, J. Cell Biol. 178 (5) (2007) 875–886.
[12] C. Leterrier, J. Potier, G. Caillol, C. Debarnot, F. Rueda Boroni, B. Dargent, Nanoscale architecture of the axon initial segment reveals an organized and robust scaffold, Cell Rep. 13 (12) (2015) 2781–2793.
[13] Y. Bekku, T. Oohashi, Neurocan contributes to the molecular heterogeneity of the perinodal ECM, Arch. Histol. Cytol. 73 (2) (2010) 95–102.
[14] G. Bruckner, S. Szeoke, S. Pavlica, J. Grosche, J. Kacza, Axon initial segment ensheathed by extracellular matrix in perineuronal nets, Neuroscience 138 (2) (2006) 365–375.
[15] A. Dityatev, C.I. Seidenbecher, M. Schachner, Compartmentalization from the outside: the extracellular matrix and functional microdomains in the brain, Trends Neurosci. 33 (11) (2010) 503–512.
[16] A. Dityatev, D.A. Rusakov, Molecular signals of plasticity at the tetrapartite synapse, Curr. Opin. Neurobiol. 21 (2) (2011) 353–359.
[17] J.W. Fawcett, T. Oohashi, T. Pizzorusso, The roles of perineuronal nets and the perinodal extracellular matrix in neuronal function, Nat. Rev. Neurosci. 20 (8) (2019) 451–465.
[18] H. Pantazopoulos, N.M. Hossain, G. Chelini, P. Durning, H. Barbas, B. Zikopoulos, S. Berretta, Chondroitin sulphate proteoglycan axonal coats in the human mediodorsal thalamic nucleus, Front. Integr. Neurosci. 16 (2022) 934764.
[19] A. Dityatev, M. Schachner, The extracellular matrix and synapses, Cell Tissue Res. 326 (2) (2006) 647–654.
[20] R. Frischknecht, K.J. Chang, M.N. Rasband, C.I. Seidenbecher, Neural ECM molecules in axonal and synaptic homeostatic plasticity, Prog. Brain Res. 214 (2014) 81–100.
[21] N. John, H. Krugel, R. Frischknecht, K.H. Smalla, C. Schultz, M.R. Kreutz, E. D. Gundelfinger, C.I. Seidenbecher, Brevican-containing perineuronal nets of extracellular matrix in dissociated hippocampal primary cultures, Mol. Cell Neurosci. 31 (4) (2006) 774–784.
[22] A. Dityatev, G. Bruckner, G. Dityateva, J. Grosche, R. Kleene, M. Schachner, Activity-dependent formation and functions of chondroitin sulfate-rich extracellular matrix of perineuronal nets, Dev. Neurobiol. 67 (5) (2007) 570–588.
[23] H. Hayani, I. Song, A. Dityatev, Increased excitability and reduced excitatory synaptic input into fast-spiking CA2 interneurons after enzymatic attenuation of extracellular matrix, Front. Cell Neurosci. 12 (2018) 149.
[24] D. Minge, O. Senkov, R. Kaushik, M.K. Herde, O. Tikhobrazova, A.B. Wulff, A. Mironov, T.H. van Kuppevelt, A. Oosterhof, G. Kochlamazashvili, A. Dityatev, C. Henneberger, Heparan sulfates support pyramidal cell excitability, synaptic plasticity, and context discrimination, Cereb. Cortex 27 (2) (2017) 903–918.
[25] I. Song, T. Kuznetsova, D. Baidoe-Ansah, H. Mirzapourdelavar, O. Senkov, H. Hayani, A. Mironov, R. Kaushik, M. Druzin, S. Johansson, A. Dityatev, Heparan sulfates regulate axonal excitability and context generalization through Ca(2+)/calmodulin-dependent protein kinase II, Cells 12 (5) (2023).
[26] E. Favuzzi, A. Marques-Smith, R. Deogracias, C.M. Winterflood, A. Sanchez-Aguilera, L. Mantoan, P. Maeso, C. Fernandes, H. Ewers, B. Rico, Activity-dependent gating of parvalbumin interneuron function by the perineuronal net protein brevican, Neuron 95 (3) (2017) 639–655, e10.
[27] S. Cichon, T.W. Muhleisen, F.A. Degenhardt, M. Mattheisen, X. Miro, J. Strohmaier, M. Steffens, C. Meesters, S. Herms, M. Weingarten, L. Priebe, B. Haenisch, M. Alexander, J. Vollmer, R. Breuer, C. Schmal, P. Tessmann, S. Moebus, H. E. Wichmann, S. Schreiber, B. Muller-Myhsok, S. Lucae, S. Jamain, M. Leboyer, F. Bellivier, B. Etain, C. Henry, J.P. Kahn, S. Heath, C. Bipolar Disorder Genome Study, M. Hamshere, M.C. O'Donovan, M.J. Owen, N. Craddock, M. Schwarz,

H. Vedder, J. Kammerer-Ciernioch, A. Reif, J. Sasse, M. Bauer, M. Hautzinger, A. Wright, P.B. Mitchell, P.R. Schofield, G.W. Montgomery, S.E. Medland, S. D. Gordon, N.G. Martin, O. Gustafsson, O. Andreassen, S. Djurovic, E. Sigurdsson, S. Steinberg, H. Stefansson, K. Stefansson, L. Kapur-Pojskic, L. Oruc, F. Rivas, F. Mayoral, A. Chuchalin, G. Babadjanova, A.S. Tiganov, G. Pantelejeva, L. I. Abramova, M. Grigoroiu-Serbanescu, C.C. Diaconu, P.M. Czerski, J. Hauser, A. Zimmer, M. Lathrop, T.G. Schulze, T.F. Wienker, J. Schumacher, W. Maier, P. Propping, M. Rietschel, M.M. Nothen, Genome-wide association study identifies genetic variation in neurocan as a susceptibility factor for bipolar disorder, Am. J. Hum. Genet. 88 (3) (2011) 372–381.

[28] X. Miro, S. Meier, M.L. Dreisow, J. Frank, J. Strohmaier, R. Breuer, C. Schmal, O. Albayram, M.T. Pardo-Olmedilla, T.W. Muhleisen, F.A. Degenhardt, M. Mattheisen, I. Reinhard, A. Bilkei-Gorzo, S. Cichon, C. Seidenbecher, M. Rietschel, M.M. Nothen, A. Zimmer, Studies in humans and mice implicate neurocan in the etiology of mania, Am. J. Psychiatry 169 (9) (2012) 982–990.

[29] T.W. Muhleisen, M. Mattheisen, J. Strohmaier, F. Degenhardt, L. Priebe, C. C. Schultz, R. Breuer, S. Meier, P. Hoffmann, G. Investigators, F. Rivandeneira, A. Hofman, A.G. Uitterlinden, S. Moebus, C. Gieger, R. Emeny, K.H. Ladwig, H. E. Wichmann, M. Schwarz, J. Kammerer-Ciernioch, R.G. Schlosser, I. Nenadic, H. Sauer, R. Mossner, W. Maier, D. Rujescu, C. Lange, R.A. Ophoff, T.G. Schulze, M. Rietschel, M.M. Nothen, S. Cichon, Association between schizophrenia and common variation in neurocan (NCAN), a genetic risk factor for bipolar disorder, Schizophr. Res. 138 (1) (2012) 69–73.

[30] M. Okamoto, J. Sakiyama, S. Mori, S. Kurazono, S. Usui, M. Hasegawa, A. Oohira, Kainic acid-induced convulsions cause prolonged changes in the chondroitin sulfate proteoglycans neurocan and phosphacan in the limbic structures, Exp. Neurol. 184 (1) (2003) 179–195.

[31] Z. Yu, Y. Han, D. Hu, N. Chen, Z. Zhang, W. Chen, Y. Xue, S. Meng, L. Lu, W. Zhang, J. Shi, Neurocan regulates vulnerability to stress and the anti-depressant effect of ketamine in adolescent rats, Mol. Psychiatry 27 (5) (2022) 2522–2532.

[32] H. Yan, X. Zhu, J. Xie, Y. Zhao, X. Liu, beta-amyloid increases neurocan expression through regulating Sox9 in astrocytes: a potential relationship between Sox9 and chondroitin sulfate proteoglycans in Alzheimer's disease, Brain Res. 1646 (2016) 377–383.

[33] A. Assmann, A. Richter, H. Schutze, J. Soch, A. Barman, G. Behnisch, L. Knopf, M. Raschick, A. Schult, T. Wustenberg, J. Behr, E. Duzel, C.I. Seidenbecher, B. H. Schott, Neurocan genome-wide psychiatric risk variant affects explicit memory performance and hippocampal function in healthy humans, Eur. J. Neurosci. 53 (12) (2021) 3942–3959.

[34] U. Dannlowski, H. Kugel, D. Grotegerd, R. Redlich, J. Suchy, N. Opel, T. Suslow, C. Konrad, P. Ohrmann, J. Bauer, T. Kircher, A. Krug, A. Jansen, B.T. Baune, W. Heindel, K. Domschke, A.J. Forstner, M.M. Nothen, J. Treutlein, V. Arolt, C. Hohoff, M. Rietschel, S.H. Witt, NCAN Cross-disorder risk variant is associated with limbic gray matter deficits in healthy subjects and major depression, Neuropsychopharmacology 40 (11) (2015) 2510–2516.

[35] H. Raum, B. Dietsche, A. Nagels, S.H. Witt, M. Rietschel, T. Kircher, A. Krug, A genome-wide supported psychiatric risk variant in NCAN influences brain function and cognitive performance in healthy subjects, Hum. Brain Mapp. 36 (1) (2015) 378–390.

[36] C. Abe, C.J. Ekman, C. Sellgren, P. Petrovic, M. Ingvar, M. Landen, Manic episodes are related to changes in frontal cortex: a longitudinal neuroimaging study of bipolar disorder 1, Brain 138 (Pt 11) (2015) 3440–3448.

[37] S.M. Strakowski, M.P. Delbello, C.M. Adler, The functional neuroanatomy of bipolar disorder: a review of neuroimaging findings, Mol. Psychiatry 10 (1) (2005) 105–116.

[38] M.A. El-Brolosy, D.Y.R. Stainier, Genetic compensation: a phenomenon in search of mechanisms, PLoS Genet. 13 (7) (2017) e1006780.

[39] A.M. Zimmer, Y.K. Pan, T. Chandrapalan, R.W.M. Kwong, S.F. Perry, Loss-of-function approaches in comparative physiology: is there a future for knockdown experiments in the era of genome editing? J. Exp. Biol. 222 (Pt 7) (2019).

[40] K.A. Giamanco, M. Morawski, R.T. Matthews, Perineuronal net formation and structure in aggrecan knockout mice, Neuroscience 170 (4) (2010) 1314–1327.

[41] B. Rudy, C.J. McBain, Kv3 channels: voltage-gated K+ channels designed for high-frequency repetitive firing, Trends Neurosci. 24 (9) (2001) 517–526.

[42] R.Q. Chen, S.H. Wang, W. Yao, J.J. Wang, F. Ji, J.Z. Yan, S.Q. Ren, Z. Chen, S. Y. Liu, W. Lu, Role of glycine receptors in glycine-induced LTD in hippocampal CA1 pyramidal neurons, Neuropsychopharmacology 36 (9) (2011) 1948–1958.

[43] L.I. Benowitz, A. Routtenberg, GAP-43: an intrinsic determinant of neuronal development and plasticity, Trends Neurosci. 20 (2) (1997) 84–91.

[44] P. Gil-Loyzaga, F. Carricondo, M.V. Bartolome, M.C. Iglesias, F. Rodriguez, J. Poch-Broto, Cellular and molecular bases of neuroplasticity: brainstem effects after cochlear damage, Acta Otolaryngol. 130 (3) (2010) 318–325.

[45] H. Ueno, K. Fujii, S. Suemitsu, S. Murakami, N. Kitamura, K. Wani, S. Aoki, M. Okamoto, T. Ishihara, K. Takao, Expression of aggrecan components in perineuronal nets in the mouse cerebral cortex, IBRo Rep. 4 (2018) 22–37.

[46] A. Willis, J.A. Pratt, B.J. Morris, Enzymatic degradation of cortical perineuronal nets reverses GABAergic interneuron maturation, Mol. Neurobiol. 59 (5) (2022) 2874–2893.

[47] V.K. Gribkoff, R.L. Pieschl, F.E. Dudek, GABA receptor-mediated inhibition of neuronal activity in rat SCN *in vitro*: pharmacology and influence of circadian phase, J. Neurophysiol. 90 (3) (2003) 1438–1448.

[48] G.A. Johnston, Advantages of an antagonist: bicuculline and other GABA antagonists, Br. J. Pharmacol. 169 (2) (2013) 328–336.

[49] J.H. Cabungcal, P. Steullet, H. Morishita, R. Kraftsik, M. Cuenod, T.K. Hensch, K. Q. Do, Perineuronal nets protect fast-spiking interneurons against oxidative stress, Proc. Natl. Acad. Sci. U. S. A. 110 (22) (2013) 9130–9135.

[50] D. Rowlands, K.K. Lensjo, T. Dinh, S. Yang, M.R. Andrews, T. Hafting, M. Fyhn, J. W. Fawcett, G. Dick, Aggrecan directs extracellular matrix-mediated neuronal plasticity, J. Neurosci. 38 (47) (2018) 10102–10113.

[51] X.H. Zhou, C. Brakebusch, H. Matthies, T. Oohashi, E. Hirsch, M. Moser, M. Krug, C.I. Seidenbecher, T.M. Boeckers, U. Rauch, R. Buettner, E.D. Gundelfinger, R. Fassler, Neurocan is dispensable for brain development, Mol. Cell Biol. 21 (17) (2001) 5970–5978.

[52] V. Mohan, E.V. Wyatt, I. Gotthard, K.D. Phend, S. Diestel, B.W. Duncan, R. J. Weinberg, A. Tripathy, P.F. Maness, Neurocan inhibits semaphorin 3F induced dendritic spine remodeling through NrCAM in cortical neurons, Front. Cell Neurosci. 12 (2018) 346.

[53] S.H. Bitzenhofer, J.A. Popplau, I. Hanganu-Opatz, Gamma activity accelerates during prefrontal development, eLife 9 (2020).

[54] J.M. Yang, J. Zhang, Y.Q. Yu, S. Duan, X.M. Li, Postnatal development of 2 microcircuits involving fast-spiking interneurons in the mouse prefrontal cortex, Cereb. Cortex. 24 (1) (2014) 98–109.

[55] C. Gottschling, D. Wegrzyn, B. Denecke, A. Faissner, Elimination of the four extracellular matrix molecules tenascin-C, tenascin-R, brevican and neurocan alters the ratio of excitatory and inhibitory synapses, Sci. Rep. 9 (1) (2019) 13939.

[56] K.K. Lensjo, M.E. Lepperod, G. Dick, T. Hafting, M. Fyhn, Removal of perineuronal nets unlocks juvenile plasticity through network mechanisms of decreased inhibition and increased gamma activity, J. Neurosci. 37 (5) (2017) 1269–1283.

[57] A.K. Saghatelyan, A. Dityatev, S. Schmidt, T. Schuster, U. Bartsch, M. Schachner, Reduced perisomatic inhibition, increased excitatory transmission, and impaired long-term potentiation in mice deficient for the extracellular matrix glycoprotein tenascin-R, Mol. Cell Neurosci. 17 (1) (2001) 226–240.

[58] A.K. Saghatelyan, A.G. Nikonenko, M. Sun, B. Rolf, P. Putthoff, M. Kutsche, U. Bartsch, A. Dityatev, M. Schachner, Reduced GABAergic transmission and number of hippocampal perisomatic inhibitory synapses in juvenile mice deficient in the neural cell adhesion molecule L1, Mol. Cell Neurosci. 26 (1) (2004) 191–203.

[59] E. Dzyubenko, M. Fleischer, D. Manrique-Castano, M. Borbor, C. Kleinschnitz, A. Faissner, D.M. Hermann, Inhibitory control in neuronal networks relies on the extracellular matrix integrity, Cell Mol. Life Sci. 78 (14) (2021) 5647–5663.

[60] D. Irala, S. Wang, K. Sakers, L. Nagendren, F.P. Ulloa Severino, D.S. Bindu, J. T. Savage, C. Eroglu, Astrocyte-secreted neurocan controls inhibitory synapse formation and function, Neuron 112 (10) (2024) 1657–1675, e10.

[61] S. Goethals, R. Brette, Theoretical relation between axon initial segment geometry and excitability, eLife 9 (2020).

[62] J. Zhang, X. Chen, M. Eaton, J. Wu, Z. Ma, S. Lai, A. Park, T.S. Ahmad, Z. Que, J. H. Lee, T. Xiao, Y. Li, Y. Wang, M.I. Olivero-Acosta, J.A. Schaber, K. Jayant, C. Yuan, Z. Huang, N.A. Lanman, W.C. Skarnes, Y. Yang, Severe deficiency of the voltage-gated sodium channel Na(V)1.2 elevates neuronal excitability in adult mice, Cell Rep. 36 (5) (2021) 109495.

[63] N. Nadella, A. Ghosh, X.P. Chu, Hyperexcitability in adult mice with severe deficiency in Na(V)1.2 channels, Int. J. Physiol. Pathophysiol. Pharmacol. 14 (1) (2022) 55–59.

[64] A. Zybura, A. Hudmon, T.R. Cummins, Distinctive properties and powerful neuromodulation of Na(v)1.6 sodium channels regulates neuronal excitability, Cells 10 (7) (2021).

[65] M. Ye, J. Yang, C. Tian, Q. Zhu, L. Yin, S. Jiang, M. Yang, Y. Shu, Differential roles of Na(V)1.2 and Na(V)1.6 in regulating neuronal excitability at febrile temperature and distinct contributions to febrile seizures, Sci. Rep. 8 (1) (2018) 753.

[66] J.P. Johnson, T. Focken, K. Khakh, P.K. Tari, C. Dube, S.J. Goodchild, J.C. Andrez, G. Bankar, D. Bogucki, K. Burford, E. Chang, S. Chowdhury, R. Dean, G. de Boer, S. Decker, C. Dehnhardt, M. Feng, W. Gong, M. Grimwood, A. Hasan, A. Hussainkhel, Q. Jia, S. Lee, J. Li, S. Lin, A. Lindgren, V. Lofstrand, J. Mezeyova, R. Namdari, K. Nelkenbrecher, N.G. Shuart, L. Sojo, S. Sun, M. Taron, M. Waldbrook, D. Weeratunge, S. Wesolowski, A. Williams, M. Wilson, Z. Xie, R. Yoo, C. Young, A. Zenova, W. Zhang, A.J. Cutts, R.P. Sherrington, S.N. Pimstone, R. Winquist, C.J. Cohen, J.R. Empfield, NBI-921352, a first-in-class, Na(V)1.6 selective, sodium channel inhibitor that prevents seizures in Scn8a gain-of-function mice, and wild-type mice and rats, eLife 11 (2022).

[67] K. Susuki, K.J. Chang, D.R. Zollinger, Y. Liu, Y. Ogawa, Y. Eshed-Eisenbach, M. T. Dours-Zimmermann, J.A. Oses-Prieto, A.L. Burlingame, C.I. Seidenbecher, D. R. Zimmermann, T. Oohashi, E. Peles, M.N. Rasband, Three mechanisms assemble central nervous system nodes of Ranvier, Neuron 78 (3) (2013) 469–482.

[68] J. Srinivasan, M. Schachner, W.A. Catterall, Interaction of voltage-gated sodium channels with the extracellular matrix molecules tenascin-C and tenascin-R, Proc. Natl. Acad. Sci. U. S. A. 95 (26) (1998) 15753–15757.

[69] M.R. Holahan, K.S. Honegger, N. Tabatadze, A. Routtenberg, GAP-43 gene expression regulates information storage, Learn. Mem. 14 (6) (2007) 407–415.

[70] J.L. Rekart, K. Meiri, A. Routtenberg, Hippocampal-dependent memory is impaired in heterozygous GAP-43 knockout mice, Hippocampus 15 (1) (2005) 1–7.

[71] K.A. Vossel, K.G. Ranasinghe, A.J. Beagle, D. Mizuiri, S.M. Honma, A.F. Dowling, S. M. Darwish, V. Van Berlo, D.E. Barnes, M. Mantle, A.M. Karydas, G. Coppola, E. D. Roberson, B.L. Miller, P.A. Garcia, H.E. Kirsch, L. Mucke, S.S. Nagarajan, Incidence and impact of subclinical epileptiform activity in Alzheimer's disease, Ann. Neurol. 80 (6) (2016) 858–870.

[72] B.F. Corbett, J.C. You, X. Zhang, M.S. Pyfer, U. Tosi, D.M. Iascone, I. Petrof, A. Hazra, C.H. Fu, G.S. Stephens, A.A. Ashok, S. Aschmies, L. Zhao, E.J. Nestler, J. Chin, DeltaFosB regulates gene expression and cognitive dysfunction in a mouse model of Alzheimer's disease, Cell Rep. 20 (2) (2017) 344–355.

[73] K. Kam, A.M. Duffy, J. Moretto, J.J. LaFrancois, H.E. Scharfman, Interictal spikes during sleep are an early defect in the Tg2576 mouse model of beta-amyloid neuropathology, Sci. Rep. 6 (2016) 20119.

[74] A.L. Eagle, P.A. Gajewski, M. Yang, M.E. Kechner, B.S. Al Masraf, P.J. Kennedy, H. Wang, M.S. Mazei-Robison, A.J. Robison, Experience-dependent induction of hippocampal DeltaFosB controls learning, J. Neurosci. 35 (40) (2015) 13773–13783.
[75] J.B. Calais, S.S. Valvassori, W.R. Resende, G. Feier, M.C. Athie, S. Ribeiro, W. F. Gattaz, J. Quevedo, E.B. Ojopi, Long-term decrease in immediate early gene expression after electroconvulsive seizures, J. Neural Transm. 120 (2) (2013) 259–266 (Vienna).
[76] R.P. Haberman, M.T. Koh, M. Gallagher, Heightened cortical excitability in aged rodents with memory impairment, Neurobiol. Aging 54 (2017) 144–151.
[77] T.W. Muhleisen, M. Leber, T.G. Schulze, J. Strohmaier, F. Degenhardt, J. Treutlein, M. Mattheisen, A.J. Forstner, J. Schumacher, R. Breuer, S. Meier, S. Herms, P. Hoffmann, A. Lacour, S.H. Witt, A. Reif, B. Muller-Myhsok, S. Lucae, W. Maier, M. Schwarz, H. Vedder, J. Kammerer-Ciernioch, A. Pfennig, M. Bauer, M. Hautzinger, S. Moebus, L. Priebe, P.M. Czerski, J. Hauser, J. Lissowska, N. Szeszenia-Dabrowska, P. Brennan, J.D. McKay, A. Wright, P.B. Mitchell, J. M. Fullerton, P.R. Schofield, G.W. Montgomery, S.E. Medland, S.D. Gordon, N. G. Martin, V. Krasnow, A. Chuchalin, G. Babadjanova, G. Pantelejeva, L. I. Abramova, A.S. Tiganov, A. Polonikov, E. Khusnutdinova, M. Alda, P. Grof, G. A. Rouleau, G. Turecki, C. Laprise, F. Rivas, F. Mayoral, M. Kogevinas, M. Grigoroiu-Serbanescu, P. Propping, T. Becker, M. Rietschel, M.M. Nothen, S. Cichon, Genome-wide association study reveals two new risk loci for bipolar disorder, Nat. Commun. 5 (2014) 3339.
[78] H. Pantazopoulos, P. Katsel, V. Haroutunian, G. Chelini, T. Klengel, S. Berretta, Molecular signature of extracellular matrix pathology in schizophrenia, Eur. J. Neurosci. 53 (12) (2021) 3960–3987.
[79] G. Matuszko, S. Curreli, R. Kaushik, A. Becker, A. Dityatev, Extracellular matrix alterations in the ketamine model of schizophrenia, Neuroscience 350 (2017) 13–22.
[80] H. Pantazopoulos, T.U. Woo, M.P. Lim, N. Lange, S. Berretta, Extracellular matrix-glial abnormalities in the amygdala and entorhinal cortex of subjects diagnosed with schizophrenia, Arch. Gen. Psychiatry 67 (2) (2010) 155–166.
[81] D.O. Perkins, C.D. Jeffries, K.Q. Do, Potential roles of redox dysregulation in the development of schizophrenia, Biol. Psychiatry 88 (4) (2020) 326–336.
[82] C. Schizophrenia, Psychiatric genome-wide association study, genome-wide association study identifies five new schizophrenia loci, Nat. Genet. 43 (10) (2011) 969–976.
[83] M.A. Ferreira, M.C. O'Donovan, Y.A. Meng, I.R. Jones, D.M. Ruderfer, L. Jones, J. Fan, G. Kirov, R.H. Perlis, E.K. Green, J.W. Smoller, D. Grozeva, J. Stone, I. Nikolov, K. Chambert, M.L. Hamshere, V.L. Nimgaonkar, V. Moskvina, M. E. Thase, S. Caesar, G.S. Sachs, J. Franklin, K. Gordon-Smith, K.G. Ardlie, S. B. Gabriel, C. Fraser, B. Blumenstiel, M. Defelice, G. Breen, M. Gill, D.W. Morris, A. Elkin, W.J. Muir, K.A. McGhee, R. Williamson, D.J. MacIntyre, A.W. MacLean, C.D. St, M. Robinson, M. Van Beck, A.C. Pereira, R. Kandaswamy, A. McQuillin, D. A. Collier, N.J. Bass, A.H. Young, J. Lawrence, I.N. Ferrier, A. Anjorin, A. Farmer, D. Curtis, E.M. Scolnick, P. McGuffin, M.J. Daly, A.P. Corvin, P.A. Holmans, D. H. Blackwood, H.M. Gurling, M.J. Owen, S.M. Purcell, P. Sklar, N. Craddock, Wellcome Trust Case Control Consortium, Collaborative genome-wide association analysis supports a role for ANK3 and CACNA1C in bipolar disorder, Nat. Genet. 40 (9) (2008) 1056–1058.
[84] K.V. Wirgenes, M. Tesli, E. Inderhaug, L. Athanasiu, I. Agartz, I. Melle, T. Hughes, O.A. Andreassen, S. Djurovic, ANK3 gene expression in bipolar disorder and schizophrenia, Br. J. Psychiatry 205 (3) (2014) 244–245.
[85] O.D. Howes, E. Shatalina, Integrating the neurodevelopmental and dopamine hypotheses of schizophrenia and the role of cortical excitation-inhibition balance, Biol. Psychiatry 92 (6) (2022) 501–513.
[86] J.C. Bartsch, B.H. Schott, J. Behr, Hippocampal dysfunction in schizophrenia and aberrant hippocampal synaptic plasticity in rodent model psychosis: a selective review, PharmacoPsychiatry 56 (2) (2023) 57–63.
[87] H. Okuda, K. Tatsumi, S. Morita, Y. Shibukawa, H. Korekane, N. Horii-Hayashi, Y. Wada, N. Taniguchi, A. Wanaka, Chondroitin sulfate proteoglycan tenascin-R regulates glutamate uptake by adult brain astrocytes, J. Biol. Chem. 289 (5) (2014) 2620–2631.
[88] Z. Su, S. Kishida, S. Tsubota, K. Sakamoto, D. Cao, S. Kiyonari, M. Ohira, T. Kamijo, A. Narita, Y. Xu, Y. Takahashi, K. Kadomatsu, Neurocan, an extracellular chondroitin sulfate proteoglycan, stimulates neuroblastoma cells to promote malignant phenotypes, Oncotarget 8 (63) (2017) 106296–106310.
[89] D.J. Taxman, L.R. Livingstone, J. Zhang, B.J. Conti, H.A. Iocca, K.L. Williams, J. D. Lich, J.P. Ting, W. Reed, Criteria for effective design, construction, and gene knockdown by shRNA vectors, BMC Biotechnol. 6 (2006) 7.
[90] J. Mitlohner, R. Kaushik, H. Niekisch, A. Blondiaux, C.E. Gee, M.F.K. Happel, E. Gundelfinger, A. Dityatev, R. Frischknecht, C. Seidenbecher, Dopamine receptor activation modulates the integrity of the perisynaptic extracellular matrix at excitatory synapses, Cells 9 (2) (2020).
[91] M.L. Seibenhener, M.W. Wooten, Isolation and culture of hippocampal neurons from prenatal mice, J. Vis. Exp. (65) (2012).
[92] D. Baidoe-Ansah, S. Sakib, S. Jia, H. Mirzapourdelavar, L. Strackeljan, A. Fischer, S. Aleshin, R. Kaushik, A. Dityatev, Aging-associated changes in cognition, expression and epigenetic regulation of chondroitin 6-sulfotransferase Chst3, Cells 11 (13) (2022).
[93] M. Meldgaard, C. Fenger, K.L. Lambertsen, M.D. Pedersen, R. Ladeby, B. Finsen, Validation of two reference genes for mRNA level studies of murine disease models in neurobiology, J. Neurosci. Methods 156 (1-2) (2006) 101–110.
[94] D.A. Fortin, M.A. Davare, T. Srivastava, J.D. Brady, S. Nygaard, V.A. Derkach, T. R. Soderling, Long-term potentiation-dependent spine enlargement requires synaptic Ca^{2+}-permeable AMPA receptors recruited by CaM-kinase I, J. Neurosci. 30 (35) (2010) 11565–11575.
[95] G. Handara, F.J.A. Hetsch, R. Juttner, A. Schick, C. Haupt, F.G. Rathjen, S. Kroger, The role of agrin, Lrp4 and MuSK during dendritic arborization and synaptogenesis in cultured embryonic CNS neurons, Dev. Biol. 445 (1) (2019) 54–67.